J. Fluid Mech. (1990), *vol.* 216, *pp.* 561–583
Printed in Great Britain

Structure of turbulence at high shear rate

By MOON JOO LEE, JOHN KIM AND PARVIZ MOIN
Center for Turbulence Research, Stanford University, Stanford, CA 94305, USA
and NASA-Ames Research Center, MS 202A-1, Moffett Field, CA 94035, USA

(Received 23 June 1989)

The structure of homogeneous turbulence subject to high shear rate has been investigated by using three-dimensional, time-dependent numerical simulations of the Navier–Stokes equations. The instantaneous velocity fields reveal that a high shear rate produces structures in homogeneous turbulence similar to the 'streaks' that are present in the sublayer of wall-bounded turbulent shear flows. Statistical quantities such as the Reynolds stresses are compared with those in the sublayer of a turbulent channel flow at a comparable shear rate made dimensionless by turbulent kinetic energy and its dissipation rate. This study indicates that high shear rate alone is sufficient for generation of the streaky structures, and that the presence of a solid boundary is not necessary.

Evolution of the statistical correlations is examined to determine the effect of high shear rate on the development of anisotropy in turbulence. It is shown that the streamwise fluctuating motions are enhanced so profoundly that a highly anisotropic turbulence state with a 'one-component' velocity field and 'two-component' vorticity field develops asymptotically as total shear increases. Because of high shear rate, rapid distortion theory predicts remarkably well the anisotropic behaviour of the structural quantities.

1. Introduction

The inner region of wall-bounded turbulent shear flows has been the subject of many investigations. It has been found that the viscous sublayer contains extremely well-organized motions. Flow visualization using the hydrogen-bubble technique by Kline *et al.* (1967) revealed that the coherent motions consist of regions of low- and high-speed fluid ('streaks'), elongated downstream and alternating in the spanwise direction. It was reported that the streaks undergo a series of dynamical processes (referred to as the bursting) during which most of turbulence production occurs (Kim, Kline & Reynolds 1971).

Outside the viscous sublayer, the streaks become less discernible and different structures persist. Theodorsen (1952, 1955) conjectured that hairpin-shaped vortices are the fundamental structures in turbulent boundary layers. Since then a number of workers have proposed organized structures and dynamical events in turbulent boundary layers, which are based on the presence of hairpin vortices. The flow visualization study of Head & Bandyopadhyay (1981) provided strong support for the existence of 'hairpin' (or 'horseshoe') vortices in turbulent boundary layers. Wallace (1982) analysed experimental results in turbulent boundary layers and proposed a hairpin vortex as the dominant flow structure originating from transverse vortex lines. Moin & Kim (1985), in their numerical investigation of a turbulent

channel flow, reported that the flow indeed contains an appreciable number of hairpins, mostly in the logarithmic layer. In a related study, Kim & Moin (1986) used conditional sampling techniques to show that the horseshoe-shaped vortical structures are associated with high Reynolds-shear stress and make a significant contribution to turbulent energy production.

There are two fundamental mechanisms by which a solid boundary affects turbulence: (i) generation of a mean velocity gradient (via the no-slip condition) which, upon interaction with turbulent shear stress, supplies energy to turbulence; and (ii) suppression (or blocking) of velocity fluctuations in its vicinity. The first effect can be regarded as dynamical and the second effect may be viewed as primarily kinematic. Here, it is hypothesized that the two effects are separate in affecting flow dynamics.

There is evidence that *both* the hairpins and streaks may be due to the effect of shear rate rather than due to the suppression of turbulence by the wall. For example, Uzkan & Reynolds (1967) conducted a shear-free turbulent boundary-layer experiment by passing grid-generated turbulence over a moving wall. When the speed of the moving wall was matched to that of the free stream, a shear-free boundary layer was produced and the near-wall streaks disappeared in the absence of mean shear. A related experiment was performed by Thomas & Hancock (1977) at a higher Reynolds number. Rogers & Moin (1987), using direct numerical simulation of a homogeneous shear flow, found the presence of hairpin vortices similar to those observed in the logarithmic layer of wall-bounded turbulent flows. However, their computed velocity patterns did not reveal elongated streaky structures; in fact, the shear rate in their computation was comparable with that in the logarithmic layer of a turbulent boundary layer. It should be noted that in a homogeneous turbulent flow there is no solid boundary to suppress velocity fluctuations.

The effect of blocking velocity fluctuations near a surface leads to a net transfer of energy from the vertical component, v, of turbulence to the horizontal components (Hunt & Graham 1978; Lee & Hunt 1989). This 'splatting' effect appears to be the reason why the vertical component of the pressure–strain-rate term, $\overline{p\,\partial v/\partial y}$, changes sign in the vicinity of the surface (Moin & Kim 1982). However, the effect of the boundary is not important for small eddies at $y \geqslant L_0$, where L_0 is the integral lengthscale.

The main objective of the present study is to examine whether homogeneous turbulence subject to high shear rate, comparable with that found in the viscous sublayer, would have streaky structures and statistical correlations similar to those found in the viscous sublayer of wall-bounded shear flows. Another objective is to examine the performance of rapid distortion theory in predicting the structure of turbulence at high shear rate. Direct numerical simulation of homogeneous turbulent shear flow was carried out to generate a database. In this study, particular emphasis is placed on the effect of shear rate on the evolution of anisotropy and time-dependent structure of turbulence. Results from the present homogeneous-flow simulation are compared with those in a turbulent channel flow computed by Kim, Moin & Moser (1987).

Dimensionless parameters that represent structures in turbulent shear flows are discussed in §2. The numerical and analytical procedures employed in this work are briefly described in §3. In §4, we present the instantaneous turbulence structures in a turbulent shear flow subject to strong shear. In §5, turbulence statistics in a homogeneous shear flow are analysed and compared with those in a turbulent

channel flow. The summary of our findings and a discussion are given in §6. In this work, x, y and z denote the streamwise, normal and spanwise coordinate directions, respectively; the corresponding fluctuating velocity components are u, v and w.

2. Structural parameters in turbulent shear flows

We consider an incompressible, turbulent shear flow subjected to a mean deformation rate in the form

$$U_{i,j} = S \begin{pmatrix} 0 & 1 & 0 \\ 0 & 0 & 0 \\ 0 & 0 & 0 \end{pmatrix}, \tag{2.1}$$

that is, the mean flow is $\boldsymbol{U} = (Sy, 0, 0)$. The 'shear rate', S, in a homogeneous turbulent flow must be *uniform* in space and *constant* in time, whereas it may be a function of the gradient-direction coordinate, y, in inhomogeneous flows. Turbulence statistics in a homogeneous turbulent flow evolve in time, and the *total shear*

$$\beta = St \tag{2.2}$$

is chosen as the dimensionless time.

The principal effects of mean shear on turbulence may be represented by the ratio of timescale of turbulence, l/q, to that of mean shear, $1/S$:

$$S^* = \frac{Sl}{q}. \tag{2.3}$$

This dimensionless parameter shall be referred to as the *shear-rate parameter*. Here, l is a lengthscale for 'energy-containing' eddies and $q = \overline{u_i u_i}^{\frac{1}{2}}$ is a turbulent velocity scale. (Repeated indices imply summation, and an overbar denotes statistical average over the three-dimensional space.) Different turbulence lengthscales were considered. For the purpose of the present investigation, we seek a dimensionless parameter whose magnitude would be a good indicator of the type of structures present in turbulent shear flows. The analysis given in the Appendix shows that a shear-rate parameter constructed with the Prandtl's mixing length or the integral scale extracted from the two-point cross-correlations between u and v is not capable of distinguishing different turbulence structures. It is concluded that the 'dissipation length', $l_d = q^3/\epsilon$ (where $\epsilon = \nu \overline{u_{i,j} u_{i,j}}$ is the dissipation rate of turbulent kinetic energy), yields a shear-rate parameter that gives a better indication of differences in turbulence structures. Note that the resulting shear-rate parameter

$$S^* = \frac{Sq^2}{\epsilon} \tag{2.4}$$

signifies the ratio of the eddy 'turnover' time, q^2/ϵ, to the timescale of mean deformation, $1/S$.

Figure 1 shows a profile of the shear-rate parameter in the near-wall region of a turbulent channel flow computed by Kim *et al.* (1987). The distance normal to the wall is made dimensionless by using the viscous lengthscale (ν/U_τ): $y^+ = yU_\tau/\nu$, where $U_\tau = \tau_w^{\frac{1}{2}}$ and $\tau_w = \nu \mathrm{d}U/\mathrm{d}y|_w$ is the kinematic wall shear stress. The shear-rate parameter attains its maximum, $S^*_{max} \approx 35$, at $y^+ \approx 10$ in the viscous sublayer and decreases to about one-sixth of the maximum in the logarithmic layer ($y^+ > 50$).

The existence of the streaky structures in a turbulent boundary layer has been

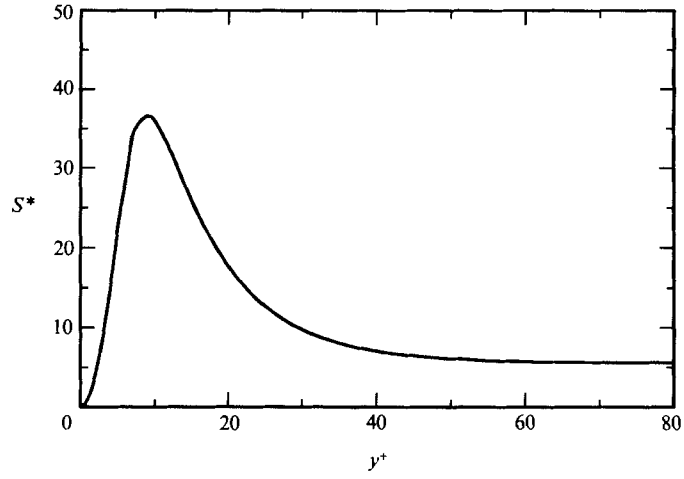

FIGURE 1. Profile of the shear-rate parameter S^* *vs.* y^+ in a turbulent channel flow (Kim *et al.* 1987), where $S^* = (\mathrm{d}U/\mathrm{d}y)\,q^2/\epsilon$, $y^+ = yU_\tau/\nu$ and $U_\tau = (\nu\,\mathrm{d}U/\mathrm{d}y|_w)^{\frac{1}{2}}$.

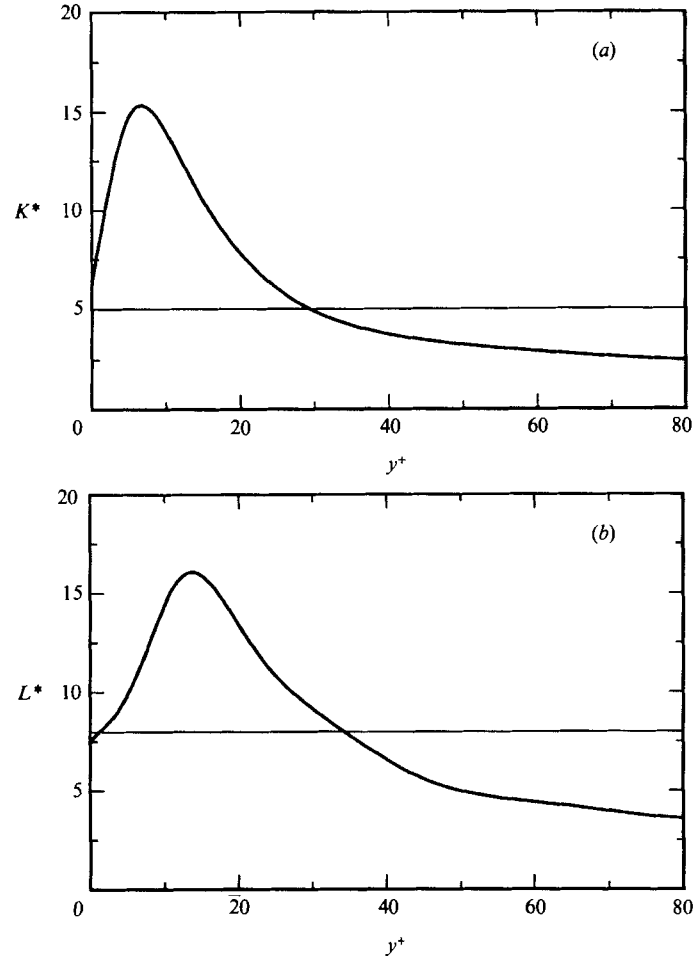

FIGURE 2. Profiles of the two dimensionless parameters used to identify streaks in a turbulent channel flow (Kim *et al.* 1987): (*a*) energy-partition parameter, $K^* = 2\overline{u^2}/(\overline{v^2}+\overline{w^2})$; (*b*) eddy-elongation parameter, $L^* = L_{uu}^{(x)}/(2L_{uu}^{(z)})$. The streak-identification criteria, $K^* > 5$ and $L^* > 8$, are satisfied by the near-wall region, $2 \leqslant y^+ \leqslant 35$.

deduced largely by flow visualization techniques. Here, we consider two quantitative measures that reflect the highly *anisotropic* nature of the streaky structures: (i) high concentration of turbulent kinetic energy in the streamwise component, u; and (ii) elongation of lengthscales associated with u in the streamwise direction. These two salient features of streaks can be quantified respectively by the dimensionless parameters

$$K^* = \frac{2\overline{u^2}}{(\overline{v^2}+\overline{w^2})}, \tag{2.5}$$

$$L^* = \frac{l_x}{l_z}, \tag{2.6}$$

where K^* and L^* are referred to as the (streamwise) *energy-partition* and *eddy-elongation parameters*, respectively. For the streamwise and spanwise lengthscales in L^*, we use the corresponding integral scales of the streamwise velocity, i.e. $l_x = L_{uu}^{(x)}$ and $l_z = 2L_{uu}^{(z)}$. (Note that $K^* = 1$ and $L^* = 1$ in isotropic turbulence.) Profiles of K^* and L^* in the channel flow are shown in figure 2. The wall-layer streaks are known to exist for $2 \leqslant y^+ \leqslant 30$–$35$, suggesting

$$K^* > 5, \quad L^* > 8 \tag{2.7}$$

as our criteria.

Turbulence statistics of primary interest in the present study are the (kinematic) Reynolds stresses, $R_{ij} = \overline{u_i u_j}$, which have a significant contribution from large-scale motions, and the vorticity correlations, $V_{ij} = \overline{\omega_i \omega_j}$, with a significant contribution from small-scale eddies ($\boldsymbol{\omega}$ is the fluctuating vorticity). In homogeneous turbulence, the dissipation rate is directly related to the vorticity variance: $\epsilon = \nu\omega'^2$ where $\omega'^2 = \overline{\omega_i \omega_i}$ (a primed quantity is the root-mean-square value). In inhomogeneous turbulence, however, this relationship holds at high Reynolds numbers only (see Tennekes & Lumley 1972, p. 88).

Other quantities of interest are the anisotropy tensors for velocity and vorticity moments

$$b_{ij} = R_{ij}/R_{kk} - \tfrac{1}{3}\delta_{ij}, \quad v_{ij} = V_{ij}/V_{kk} - \tfrac{1}{3}\delta_{ij}. \tag{2.8}$$

The overall degree of anisotropy in the Reynolds-stress and vorticity correlation tensors may be measured by the second invariants of the anisotropy tensors:

$$\mathrm{II}_b = -\tfrac{1}{2}b_{ij}b_{ji}, \quad \mathrm{II}_v = -\tfrac{1}{2}v_{ij}v_{ji}. \tag{2.9}$$

These measures for the Reynolds-stress tensor were first introduced by Lumley (see Lumley 1978). The reader is also referred to Lee (1985, §2.5) for a detailed discussion on the properties of the anisotropy tensors and their invariants.

3. Numerical simulation and rapid distortion theory

3.1. *Numerical simulation*

The direct numerical simulation (DNS, hereinafter) reported here was carried out on a Cray X-MP computer with a pseudo-spectral code developed by Rogallo (1981) for homogeneous turbulence. The algorithm employs a linear transformation by which the flow variables of the Navier–Stokes equations are computed on a grid rotating and deforming with the gradient of an imposed mean flow (for details of the algorithm, see Rogallo 1981; Lee 1985). In such a simulation, as the grid becomes greatly distorted, the range of lengthscales of turbulence in some direction may not

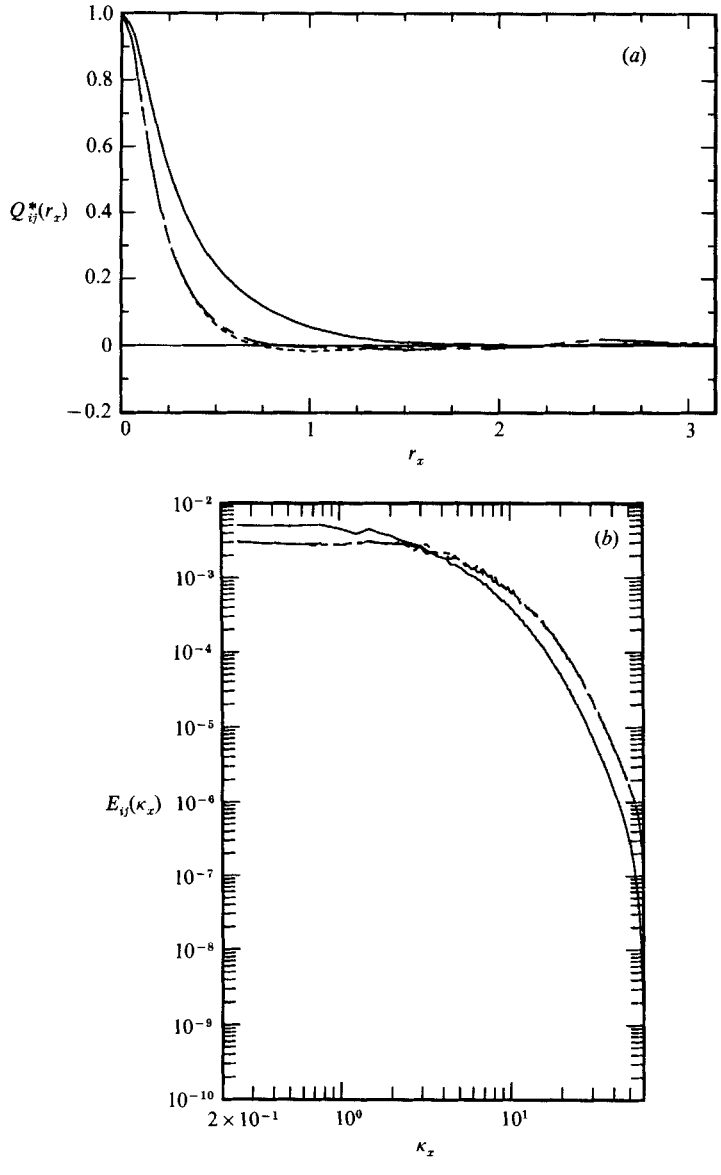

FIGURE 3. Initial isotropic turbulent field for the shear-flow simulations: (*a*) two-point velocity correlations, $Q_{ij}^*(r_x)$, showing that the computational domain is sufficiently larger than the correlation scales; (*b*) one-dimensional energy spectra, $E_{ij}(\kappa_x)$, showing the general adequacy of the grid resolution. ——, $i,j = 1,1$; – – – –, $i,j = 2,2$; — — —, $i,j = 3,3$.

be contained within the resolved range. This problem is usually avoided by remeshing of the distorted grid (at regular intervals), which, however, introduces alias errors. The resulting alias errors may be removed by a combination of phase shift and truncation of high wavenumbers, the latter of which in effect leads to loss of energy (and dissipation rate), on the order of 1–5% if shear is weak.

When turbulence is subjected to high shear rate, the loss of energy (and dissipation rate) is rather substantial: 20–40%. However, because strong shear gives rise to a growth of turbulence lengthscales with the mean flow, the grid distortion is expected

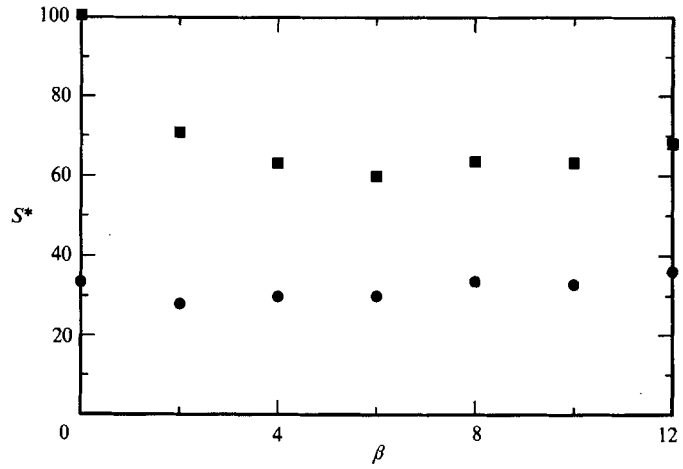

FIGURE 4. Variation of the shear-rate parameter, S^*, with total shear, β, in homogeneous turbulent shear flows (DNS) for different initial values: ●, $S_0^* = 33.5$; ■, $S_0^* = 100$.

to be less of a concern than in the case of weak shear where small-scale eddies are not well resolved since they remain more isotropic. For these reasons, in the present shear-flow simulations we chose not to remesh the grid.

The computations were conducted on a mesh with 8.4×10^6 grid points, $512 \times 128 \times 128$ in the streamwise (x), normal (y) and spanwise (z) directions, respectively. A uniform grid spacing was used in all the three directions. The computational domain is four times larger in the streamwise direction to accommodate elongated eddies that form owing to high shear rate. However, beyond some total shear at which the streamwise extent of the eddies has grown comparable to the domain, the numerical simulation will suffer from insufficient resolution.

The initial velocity field for the shear-flow simulations was obtained from a separate isotropic-decay run (without mean velocity gradients) in which the velocity-derivative skewness, $\overline{u_{,x}^3}/\overline{u_{,x}^2}^{\frac{3}{2}}$, had attained a value of -0.47, in good agreement with the experimental data (for a succinct review, see Tavoularis, Bennett & Corrsin 1978). The initial anisotropy was negligibly small: $|\mathrm{II}_b| \approx 4 \times 10^{-5}$ and $|\mathrm{II}_v| \approx 8 \times 10^{-7}$. The two-point correlations and one-dimensional spectra of velocity components of the developed isotropic field are shown in figure 3. The computational domain is about 16 times larger than the distance at which the two-point correlations vanish, illustrating that the domain is sufficiently large. The energy spectra show that the energy density contained at high wavenumbers is several decades lower than that at low wavenumbers, indicating the general adequacy of the grid resolution.

Because it was not obvious *a priori* what shear rate, S, in a homogeneous shear flow would, at the developed stage, result in a value of S^* comparable with the maximum value in the channel flow ($S_{\max}^* \approx 35$ at $y^+ \approx 10$, see figure 1), it was necessary to try several values of the shear rate. Figure 4 shows the evolution of the shear-rate parameter (or equivalently, the turbulence timescale, q^2/ϵ, since S is constant) for two numerical simulations conducted at different initial values, $S_0^* = 33.5$ and 100. In each case, there is a transient period associated with the response to imposed mean shear followed by a period of slow monotonic growth; the period of the transient behaviour is longer in the higher shear-rate case ($S_0^* = 100$). The case with $S_0^* = 33.5$ was chosen for a detailed study, because of its better agreement with the value of S^* at $y^+ \approx 10$ in the turbulent channel flow (cf. figure 1).

The grid spacing used in the selected shear-flow simulation ($S_0^* = 33.5$) was $\Delta \approx 4(\nu/S)^{\frac{1}{2}}$. The turbulence Reynolds number defined as $Re_T = q^4/(\nu\epsilon)$ ranged from 300 to 2400 for $\beta = 0$–16 (note that $Re_T = 9u'^4/(\nu\epsilon)$ in isotropic turbulence). The Reynolds number, $Re_\lambda = q\lambda/\nu$, based on the longitudinal Taylor microscale, $\lambda = (\overline{u^2}/\overline{u_{,x}^2})^{\frac{1}{2}}$, ranged from 40 to 400.

3.2. *Rapid distortion theory*

Rapid distortion theory (RDT, hereinafter) is useful for understanding the dynamics and structures of turbulence subjected to high mean-field deformation rates (see, for example, Hunt 1978 for a review). When the mean deformation is very rapid compared to the turbulence timescale (i.e. $S^* \gg 1$), the governing equations in homogeneous turbulence can be linearized by neglecting the nonlinear (turbulent inertial) terms:

$$\frac{\partial \boldsymbol{u}}{\partial t} + (\boldsymbol{U}\cdot\boldsymbol{\nabla})\,\boldsymbol{u} = -\frac{1}{\rho}\boldsymbol{\nabla}p + \nu\boldsymbol{\nabla}^2\boldsymbol{u} - (\boldsymbol{u}\cdot\boldsymbol{\nabla})\,\boldsymbol{U}. \tag{3.1}$$

In a homogeneous shear flow, the uniform mean shear asymptotically aligns wavenumber vectors in the vertical (y) direction and gives rise to a linear growth of its magnitude with the total shear. Analytical solutions for the Fourier amplitudes, $\hat{\boldsymbol{u}}(\boldsymbol{\kappa}, t)$, of velocity fluctuations can be obtained in closed form as functions of the total shear and their initial values, $\hat{\boldsymbol{u}}(\boldsymbol{\kappa}, 0)$ (Moffatt 1967; Townsend 1970). Statistical quantities such as the energy spectra and correlations can then be obtained directly from $\hat{\boldsymbol{u}}(\boldsymbol{\kappa}, t)$. The last term, $(\boldsymbol{u}\cdot\boldsymbol{\nabla})\,\boldsymbol{U} = (Sv, 0, 0)$, in the linearized equation represents distortion of turbulence by mean vorticity, a principal mechanism by which kinetic energy is supplied from the mean to turbulence in a shear flow.

Turbulence statistics predicted by RDT are compared with those of the numerical simulation to examine the relevance of the theory. A unique feature of the application of RDT in the present work is the combination of DNS and RDT which allows the study of *instantaneous* flow fields, unlike previous studies where only the statistical quantities could be examined. The initial conditions for the Fourier *velocity* components in our RDT calculation were the same (developed) isotropic turbulent field used to initialize the shear-flow simulations. We have computed instantaneous turbulence fields using RDT in an attempt to elucidate the essential mechanism(s) associated with the formation of the streaks in turbulent shear flow.

4. Instantaneous turbulence structures

To examine the effect of shear rate on instantaneous turbulence structures, contours of the streamwise component of velocity fluctuations in a homogeneous shear flow at a low shear rate ($S^* \approx 9$, Rogers & Moin 1987) are plotted on a horizontal (z, x)-plane in figure 5. Flow structures at this low shear rate are not highly elongated in the streamwise direction. Rogers & Moin showed that the flow field contains a number of hairpin vortices. Note that the value of S^* for this field is comparable with that in the logarithmic layer of a turbulent channel flow ($S^* \approx 7$) as shown in figure 1. Here and in the following contour plots, tick marks on the inner axes denote the location of the grid points, and the outer axes show the extent of a domain in the viscous lengthscale, $(\nu/S)^{\frac{1}{2}}$ (analogous to the wall unit, ν/U_τ, for wall-bounded flows); each tick mark represents 20 viscous units.

In figures 6 and 7, plots of u-contours in the homogeneous turbulent shear flow at the high shear rate are shown at times $\beta = 4$ ($S^* = 29.8$) and 8 ($S^* = 33.6$),

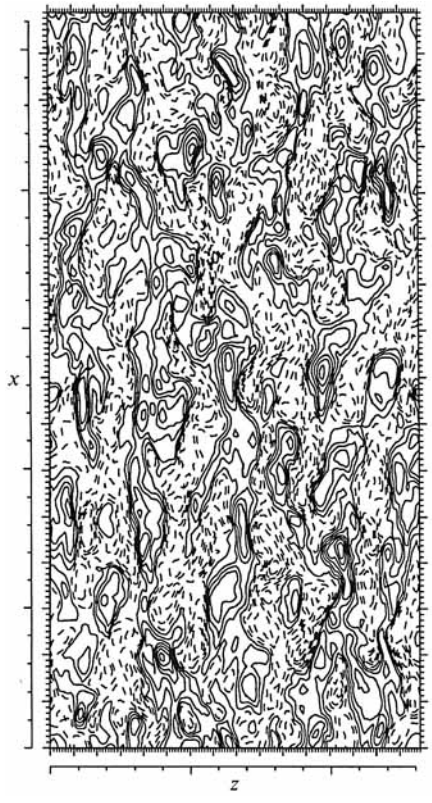

FIGURE 5.

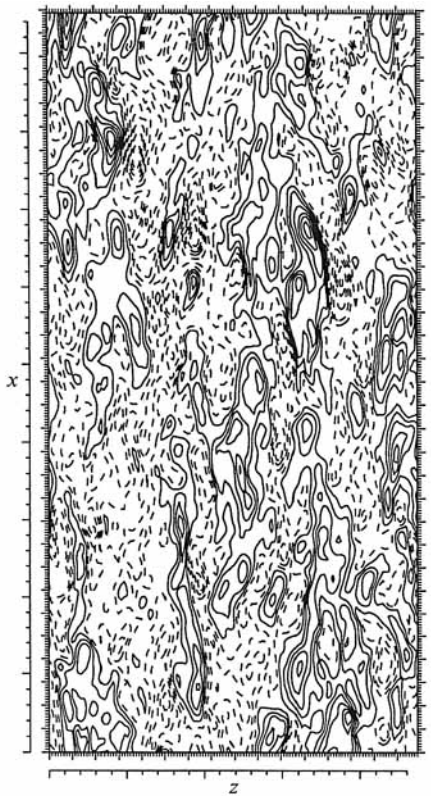

FIGURE 6.

FIGURE 5. Contours of the streamwise turbulent velocity in a homogeneous turbulent flow at a low shear rate ($S^* = 8.65$, Rogers & Moin 1987): $\beta = 8$. ——, $u \geqslant 0$; – – –, $u < 0$. Each tick mark on the outer axes represents 20 viscous units, $(\nu/S)^{\frac{1}{2}}$. In the presence of weak shear, the flow structures are not highly elongated.

FIGURE 6. Contours of the streamwise turbulent velocity in a homogeneous turbulent flow (DNS) subject to a high shear rate ($S^* = 29.8$): $\beta = 4$. ——, $u \geqslant 0$; – – –, $u < 0$. Each tick mark on the outer axes represents 20 viscous units, $(\nu/S)^{\frac{1}{2}}$. At an early time, the strong shear produces structures somewhat elongated in the streamwise direction.

respectively. The spanwise (z) and streamwise (x) dimensions of the figures are about 500 and 1000 in the viscous length units, respectively. (Only half of the streamwise extent of the computational domain is shown in these figures.) At the earlier time ($\beta = 4$, figure 6), the structures are somewhat elongated in the streamwise direction, and at the later time ($\beta = 8$, figure 7), the structures become highly elongated in the flow direction and narrow in the spanwise direction.

Figure 8 shows contours of instantaneous u from a field obtained by RDT, with the same initial velocity field as for the DNS fields in figures 6 and 7. The shear-rate parameter for this RDT field ($\beta = 8$) is $S^* = 37.9$. The gross feature of the streaky structures in the DNS field (figure 7) is also discernible in the RDT field, indicating that the essential mechanism responsible for formation of the streaks is contained in the linear theory.

To compare to wall-bounded shear flows, contours of the streamwise velocity component at $y^+ \approx 10$ in a turbulent channel flow (Kim *et al.* 1987) are plotted in figure 9. The spanwise and streamwise dimensions are about 500 and 1000 wall units

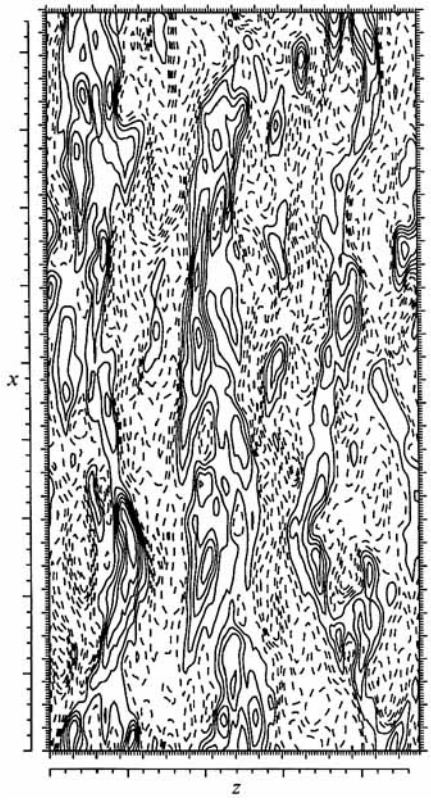

FIGURE 7.

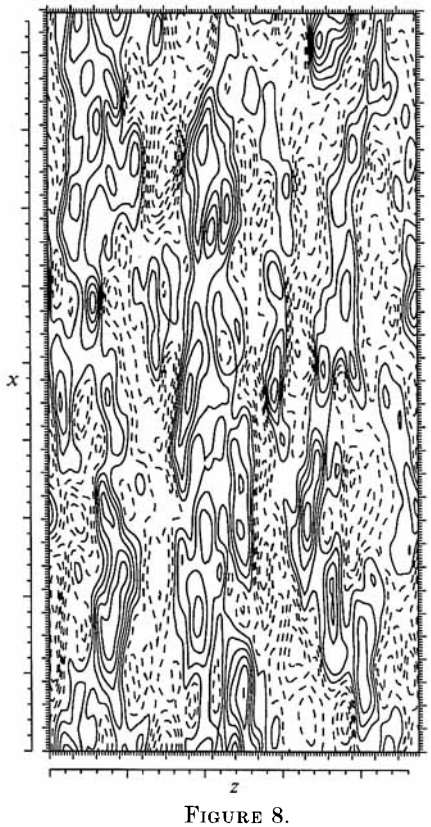

FIGURE 8.

FIGURE 7. Contours of the streamwise turbulent velocity in a homogeneous turbulent flow (DNS) subject to a high shear rate ($S^* = 33.6$): $\beta = 8$. ——, $u \geqslant 0$; – – –, $u < 0$. Each tick mark on the outer axes represents 20 viscous units, $(\nu/S)^{\frac{1}{2}}$. As total shear increases, the structures become highly elongated in the flow direction and narrow in the spanwise direction owing to the strong shear.

FIGURE 8. Contours of the streamwise turbulent velocity in a homogeneous turbulent shear flow predicted by RDT: $\beta = 8$, $S^* = 37.9$. ——, $u \geqslant 0$; – – –, $u < 0$. Each tick mark on the outer axes represents 20 viscous units, $(\nu/S)^{\frac{1}{2}}$. Note the close similarity between the instantaneous flow structures in the DNS and RDT fields (cf. figure 7).

(ν/U_τ), respectively. It can be seen that there is a resemblance between the flow patterns in figures 7 and 9. However, the eddies in the homogeneous flow are less streaky than those in the sublayer of the channel.

The mean spacing between the streaks in the sublayer of a turbulent boundary layer is usually inferred from the two-point autocorrelation of the streamwise velocity with spanwise separations, $Q^*_{uu}(r_z)$. Since the low- and high-speed streaks alternate in the spanwise direction, the mean streak spacing is about twice the separation at which the minimum value (negative) of $Q^*_{uu}(r_z)$ occurs. The mean spacing of the sublayer streaks in figure 9 ($y^+ \approx 10$) was estimated as $\lambda_z^+ = \lambda_z U_\tau/\nu \approx 100$ (Kim *et al.* 1987), in good agreement with experimentally observed values (see e.g. Smith & Metzler 1983). If the mean streak spacing is scaled by a viscous length, $(\nu/S)^{\frac{1}{2}}$, based on the local mean shear rate ($S = \mathrm{d}U/\mathrm{d}y$), then $\lambda_z^* = \lambda_z/(\nu/S)^{\frac{1}{2}} \approx 110$–$200$ in the region where $S^* > 20$ ($5 \leqslant y^+ \leqslant 15$). Figure 10 shows the two-point correlation function, $Q^*_{uu}(r_z)$, for the homogeneous shear flow that contains the streaky structures as shown in figure 7. The flat region (instead of the usual sharp

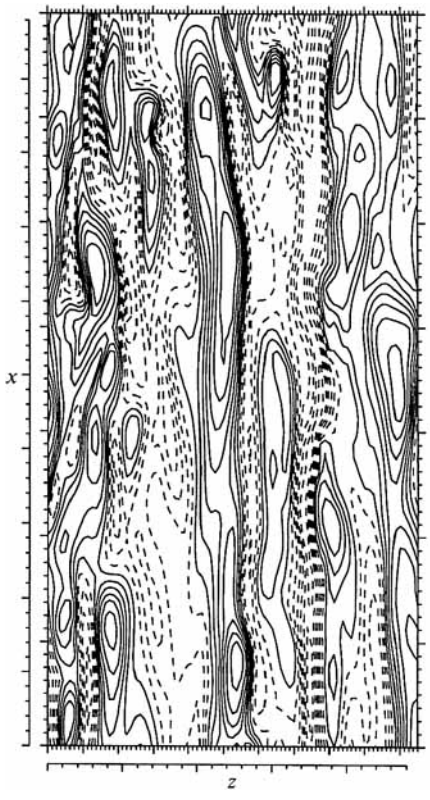

FIGURE 9. Contours of the streamwise turbulent velocity in a turbulent channel flow (Kim *et al.* 1987): $y^+ \approx 10$ ($S^* = 35.1$). ——, $u \geqslant 0$; – – – –, $u < 0$. Each tick mark on the outer axes represents 20 wall units, ν/U_τ.

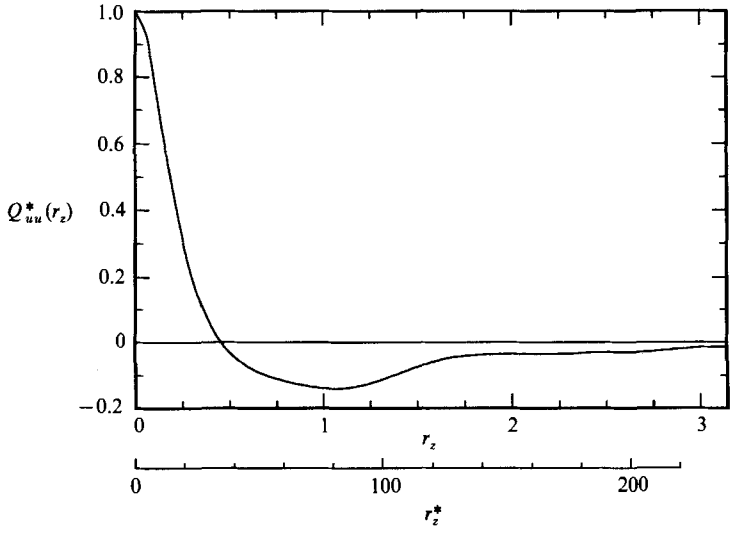

FIGURE 10. Spanwise two-point autocorrelation function of the streamwise velocity, $Q^*_{uu}(r_z)$, for homogeneous shear turbulence (DNS) subjected to a high shear rate: $\beta = 8$.

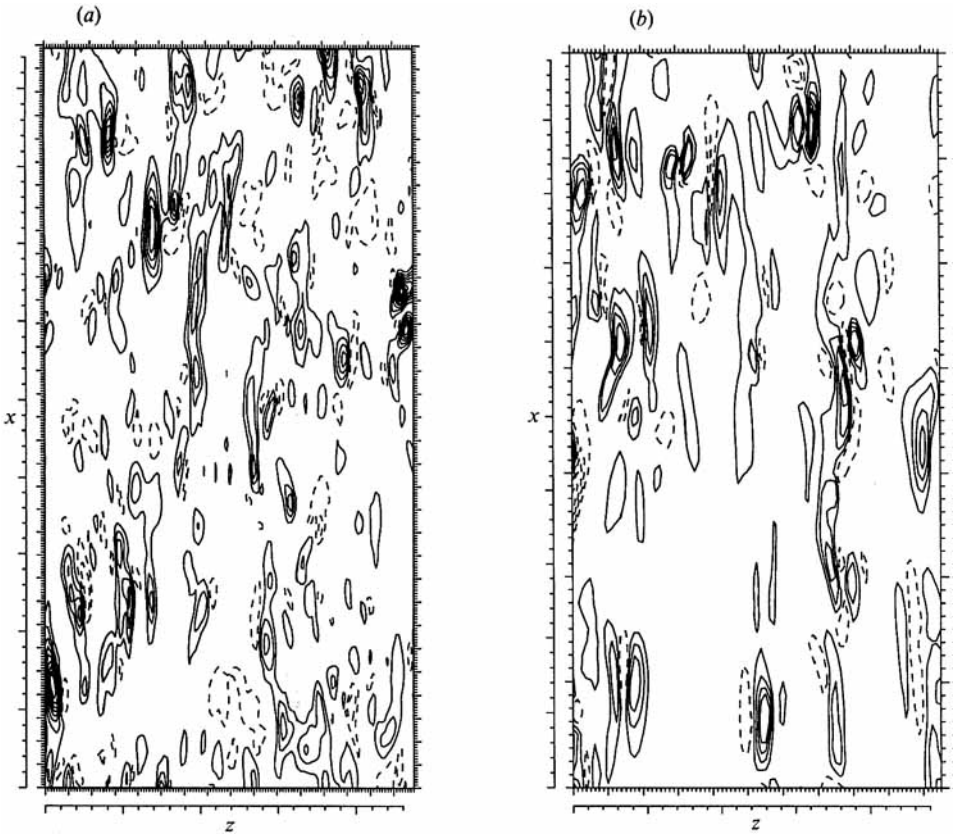

FIGURE 11. Comparison of contours of instantaneous uv: (*a*) homogeneous turbulent shear flow (DNS), $\beta = 8$, $S^* = 33.6$; (*b*) turbulent channel flow (Kim *et al.* 1987), $y^+ \approx 10$, $S^* = 35.1$. ——, $-uv \geqslant 0$; – – – –, $-uv < 0$. Each tick mark on the outer axes represents (*a*) 20 viscous units, $(\nu/S)^{\frac{1}{2}}$; and (*b*) 20 wall units, ν/U_τ, respectively.

minimum for a wall-bounded turbulent flow) of negative values of the two-point correlation indicates the existence of a wide distribution of spacings between streaks in the homogeneous shear flow. The mean streak spacing estimated from the figure varies from about 120 to 200 in units of the viscous lengthscale, $(\nu/S)^{\frac{1}{2}}$, comparable with the range of values in the sublayer of a wall-bounded flow.

But, the above agreement between the two flows of the mean streak spacing in the viscous length units is coincidental at large, because in inhomogeneous shear flow the flow geometry, such as non-uniform mean velocity profile and/or flow width, primarily sets a lengthscale of the dominant motion, while in homogeneous shear flow the initial energy spectra determine the scales of turbulent eddies that develop in time (see the inhomogeneous RDT analysis of a uniform-shear boundary layer by Lee & Hunt 1989). The more important implication of the similarity in turbulence structure between the two flows is that the dominant mechanism in the production (and maintenance) of the preferred structures (i.e. streaks) in all turbulent shear flows at high shear rate is a selective amplification of eddies primarily by the linear interaction with mean shear, and the essence of such a mechanism is accurately contained in RDT.

It is of great interest to examine the spatial distribution of the turbulence production term, $-\overline{uv}\,\mathrm{d}U/\mathrm{d}y$, in the two flows. In figure 11, contours of instantaneous uv are shown in horizontal planes in the homogeneous and channel flows. The most conspicuous feature of the uv-distribution is that regions of high Reynolds-shear stress (and turbulence production) in both flows are very intermittent and localized in space.

Contours of the streamwise velocity, u (and uv), in the vertical (x, y)-plane of the homogeneous shear flow (not shown here) indicate that the vertical extent of the streaks is very narrow compared even with the spanwise extent and that the streaks have a shallow angle (less than 10° at $\beta = 8$) with the flow direction, similar to those in the sublayer of wall-bounded flows. The 'flat-eddy' model of Landahl (1977, 1980), proposed based on the large (streamwise to vertical) aspect ratio and the shallow inclination of the wall-layer eddies, has shown how an inviscid, linear mechanism leads to formation of longitudinal streaks (or internal shear layers).

In comparing the instantaneous structures, however, we do not contend that the two flows are similar in every detail. In order to see how the distribution of velocity fluctuations is different (or similar) in the two flows, we examine higher-order statistics. In the homogeneous flow (DNS and RDT), the streamwise component of velocity fluctuation, u, has a skewness factor close to zero (0.01–0.02) and a flatness factor of about three (i.e. same as for a Gaussian distribution); the other components also have almost Gaussian distributions. In the channel flow, however, the skewness and flatness factors of u are 0.1 and 2.2, respectively, and those of v are -0.2 and 7.9 at $y^+ \approx 10$ (Kim *et al.* 1987). Since the gross feature of the instantaneous structures of turbulence at high shear rate has an apparent similarity, the departure from Gaussianity of velocity distribution in the channel flow is due to the presence of a solid boundary. The inhomogeneity resulting from the suppression effect (absent in homogeneous turbulence) gives rise to transport, among other things, which requires non-zero third moments.

5. Turbulence statistics

5.1. *Homogeneous shear turbulence*

The time history of the Reynolds-stress anisotropy tensor is shown in figure 12. The most distinguished feature in the energy partition among components is that turbulent kinetic energy is increasingly concentrated in the streamwise component (b_{11}), suggesting that prolonged shear would produce, in the limit $\beta \to \infty$, a 'one-component' turbulence ($u_2/u_1 = u_3/u_1 = 0$ or, equivalently, $b_{11} = \frac{2}{3}, b_{22} = b_{33} = -\frac{1}{3}$; see also figure 17). The shear-stress component, $|b_{12}|$, first increases to a maximum (0.15 ± 0.02) at around $\beta = 2$, and then gradually decreases owing to a rapid growth of the turbulent kinetic energy relative to that of the shear-stress magnitude. The RDT results in the figure are in good agreement with the simulation data for all the components, indicating that the energy distribution among the components at high shear rate is accurately represented by the linear theory.

Variation of the energy-partition parameter, $K^* = (\frac{2}{3} + 2b_{11})/(\frac{2}{3} - b_{11})$, with the total shear is shown in figure 13 for homogeneous shear flows at different shear rates. It is clearly shown that a strong shear leads to a much higher value of K^*. Note that the first criterion for identification of streaks, i.e. $K^* > 5$, is not satisfied for any values of the total shear in the low shear-rate case, in accord with the observation that this flow does not contain streaky structures (Rogers & Moin 1987). In the

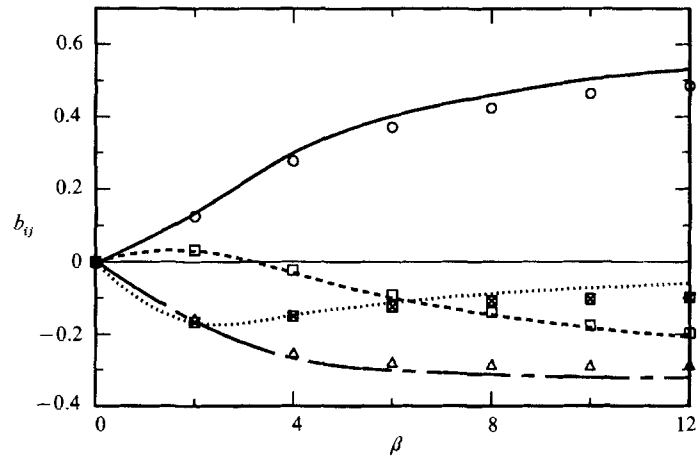

FIGURE 12. Comparison between DNS and RDT of the development of the Reynolds-stress anisotropy in homogeneous turbulent shear flow. Symbols are from DNS: ○, b_{11}; △, b_{22}; □, b_{33}; ⊠, b_{12}. Lines are from RDT: ——, b_{11}; – – –, b_{22}; – – –, b_{33}; ....., b_{12}.

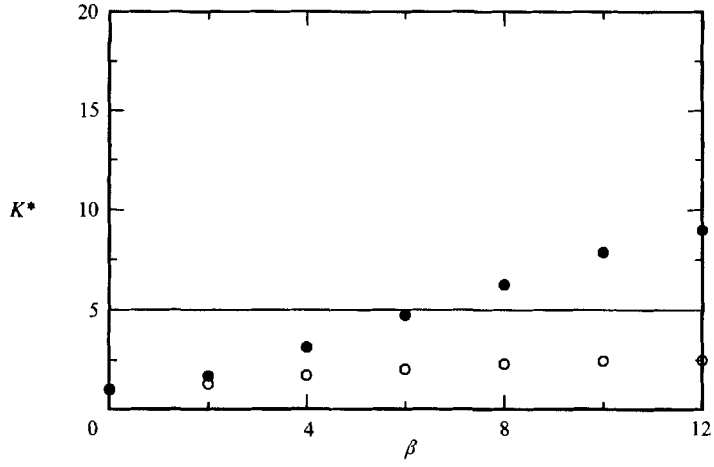

FIGURE 13. Evolution of the energy-partition parameter, K^*, in homogeneous turbulent flows at different shear rates. ○, low shear-rate case ($S_0^* \approx 5$, DNS); ●, high shear-rate case ($S_0^* \approx 34$, DNS).

presence of a strong shear, however, K^* becomes as high as 10 in the developed stage ($\beta \geqslant 8$), exceeding the threshold value of 5.

The evolution of the streamwise integral lengthscale of the streamwise velocity, defined as $L_{uu}^{(x)} = \pi E_{uu}(\kappa_x = 0)/\overline{u^2}$, is shown in figure 14. Both the DNS and RDT results show that the integral scale grows monotonically with the total shear in the presence of a high shear rate. Since turbulent kinetic energy is mostly concentrated in the streamwise component in this flow, the longitudinal integral scale, $L_{uu}^{(x)}$, can be also viewed as representing the streamwise scale of the energy-containing eddies. This implies that large eddies in a turbulent shear flow are continuously elongated in the flow direction.

Figure 15 shows the temporal development of the lengthscale ratio of eddies at

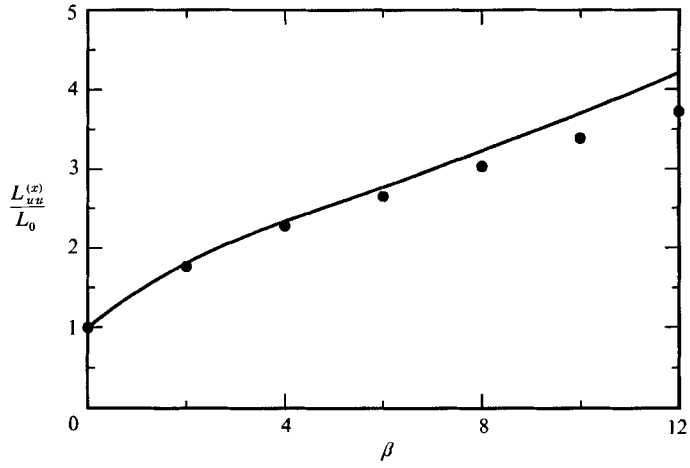

FIGURE 14. Comparison between DNS and RDT of growth of the longitudinal integral scale, $L_{uu}^{(x)}/L_0$, in homogeneous turbulent shear flow (L_0 is the initial value): ●, DNS; ——, RDT.

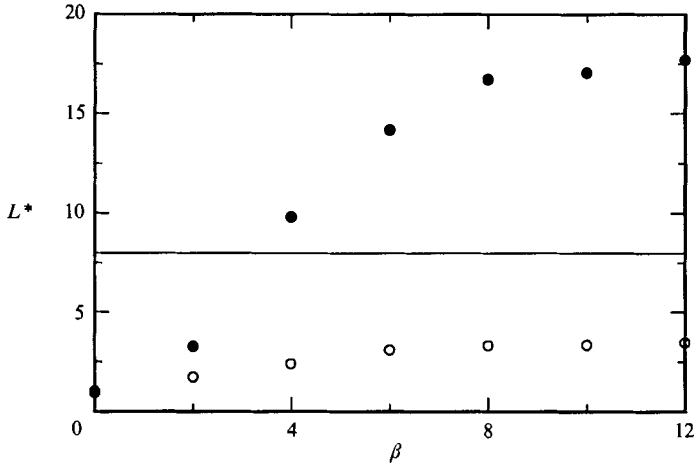

FIGURE 15. Evolution of the eddy-elongation parameter, L^*, in homogeneous turbulent flows at different shear rates: ○, low shear-rate case ($S_0^* \approx 5$, DNS); ●, high shear-rate case ($S_0^* \approx 34$, DNS).

high and low shear rates. Strong shear produes eddies of high aspect ratio, which indicates the development of streaky structures in the flow. Application of the second criterion alone, $L^* = L_{uu}^{(x)}/(2L_{uu}^{(z)}) > 8$, suggests that the streaky structures would appear for $\beta \geqslant 4$. However, combination of the two criteria predicts that streaks are identifiable for $\beta \geqslant 8$, which is entirely consistent with the appearance of streaks at around $\beta = 8$ as shown in §4 (cf. figures 6 and 7).

In figure 16, the evolution of anisotropy of the small scales (vorticity) is shown. After the initial transient period, the spanwise component of vorticity fluctuations (v_{33}) dominates, and the streamwise fluctuation becomes negligible ($v_{11} \to -\frac{1}{3}$, or $\omega_1'/\omega_3' \to 0$). However, the normal component (v_{22}) is significant, indicating that the small-scale field would reach a 'two-component' state in the limit of large β. The cross-correlation component in the vorticity (v_{12}) shows a trend similar to that of the

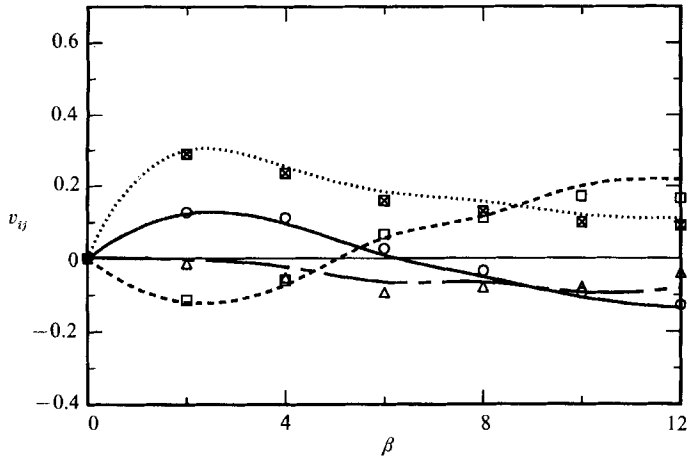

FIGURE 16. Comparison between DNS and RDT of the development of the vorticity anisotropy in homogeneous turbulent shear flow. Symbols are from DNS: ○, v_{11}; △, v_{22}; □, v_{33}; ⊠, v_{12}. Lines are from RDT: ——, v_{11}; – – –, v_{22}; – – –, v_{33}; ....., v_{12}.

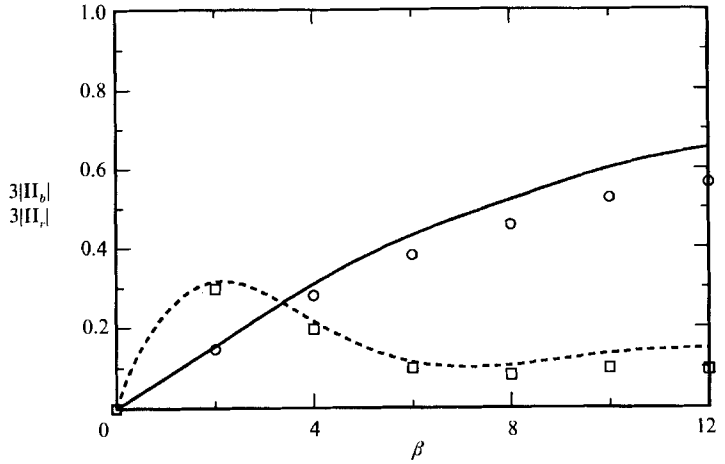

FIGURE 17. Comparison between DNS and RDT of the large- and small-scale anisotropy of homogeneous turbulent shear flow. Symbols are from DNS: ○, $3|\mathrm{II}_b|$; □, $3|\mathrm{II}_v|$. Lines are from RDT: ——, $3|\mathrm{II}_b|$; – – –, $3|\mathrm{II}_v|$.

Reynolds-stress field (b_{12}). Agreement between the simulation and RDT in the vorticity anisotropy evolution is not as good as for the Reynolds-stress field, indicating the inadequacy of RDT for the small-scale motions.

Overall anisotropy levels in the large- and small-scale turbulence are compared in figure 17. The large-eddy anisotropy, $|\mathrm{II}_b|$, is much larger than the small-scale anisotropy, $|\mathrm{II}_v|$, except in the initial transient period. The monotonic growth of $|\mathrm{II}_b|$ is a direct consequence of the dominance of the streamwise velocity component in this flow. It is shown in the figure that RDT qualitatively predicts the monotonic growth of $|\mathrm{II}_b|$. Also, RDT correctly predicts a maximum of $|\mathrm{II}_v|$ near $\beta = 2$ followed by a decrease.

Some earlier attempts to describe laboratory experiments on homogeneous turbulence using RDT were not satisfactory, because (i) mean strain rate in the experiments was not high enough for RDT to be applied, i.e. $S^* \sim O(1)$; (ii) the high

	Channel†	Homogeneous shear flow (DNS)		
	$y^+ \approx 10$	$\beta = 4$	$\beta = 8$	$\beta = 12$
S^*	35.1	29.8	33.6	36.2
Re_T	454.0	513.0	1230.0	2400.0
S/ω'	1.65	1.32	0.960	0.738
$\overline{u^2}/q^2$	0.886	0.610	0.758	0.818
$\overline{v^2}/q^2$	0.013	0.081	0.049	0.047
$\overline{w^2}/q^2$	0.100	0.309	0.194	0.135
$-\overline{uv}/q^2$	0.054	0.151	0.108	0.100

† Database generated by Kim *et al.* (1987).

TABLE 1. Comparison of turbulence statistics at high shear rate

degree of anisotropy in 'initial' grid turbulence (for example, $\overline{u_2^2}/\overline{u_1^2} \approx 1.45$ in the case of Tucker & Reynolds 1968) was not properly accounted for in the use of RDT; and (iii) the homogeneity of the downstream turbulence (and hence the profile of mean velocity) was affected by the rapid growth of the boundary-layer thickness and some exit conditions (see e.g. Reynolds & Tucker 1975). Together with the close agreement in the present study, the almost perfect agreement in the structural quantities between DNS (at low Reynolds numbers) with $S^* \gg 1$ and *inviscid* RDT of homogeneous turbulence subject to irrotational strains (Lee 1985, 1989) indicates that, if $S^* \gg 1$, then the flow dynamics is governed principally by an inviscid, linear process and there is little effect of Reynolds number. But, if S^* is low, the agreement is better at low Reynolds numbers because of the smaller effects of nonlinear processes at the smallest scales.

5.2. *Comparison with a turbulent channel flow*

In table 1, turbulence statistics in the simulated homogeneous shear flow at $\beta = 4$, 8 and 12 ($S_0^* = 33.5$) are compared with those at $y^+ \approx 10$ of a channel flow (Kim *et al.* 1987). At this location, the value of S^* in the turbulent channel flow is comparable with those in the homogeneous shear flow. In the homogeneous shear flow, the turbulence Reynolds number, $Re_T = q^4/(\nu\epsilon)$, increases with shear, indicating a rapid growth of the 'large-eddy' timescale (q^2/ϵ or eddy 'turnover' time) compared to the 'small-eddy' timescale (ω'). Note that, in homogeneous turbulence, the Reynolds number is the square of the ratio of the two timescales: $Re_T = (\omega' q^2/\epsilon)^2$. On the other hand, S/ω' denotes the ratio of the timescale of fine-scale turbulence to that of the mean field. Table 1 shows that the values of S and ω' are of the same order both in the sublayer of the channel flow and in the homogeneous flow. The ratio is significantly lower ($S/\omega' \approx 0.25$) in the logarithmic layer of the channel flow, where S^* is lower.

Comparison of the Reynolds-stress anisotropy between the two flows shows a certain degree of similarity and difference: $u'/v' \approx 8$ at $y^+ \approx 10$ in the channel and $u'/v' \approx 4$ for $\beta \geqslant 8$ in the homogeneous flow. The significant enhancement of the streamwise velocity component and reduction of the normal component by shear is a common characteristic of both shear flows. The higher value of u'/v' in the sublayer of the channel flow is due to the presence of a solid boundary which suppresses the vertical component of velocity fluctuation in its vicinity, an effect absent in homogeneous turbulence (Hunt 1984; Lee & Hunt 1989). Nonetheless, the high value

of u'/v' in regions slightly away from the boundary ($10 \leqslant y^+ \leqslant 30$) is primarily due to the shear effect, i.e. high shear rate alone can lead to such differences between the streamwise and normal velocity fluctuations.

6. Summary and discussion

The instantaneous turbulence structures and temporal development of turbulence statistics in a homogeneous shear flow at a high shear rate have been analysed by using results obtained from a direct numerical simulation. The results have been compared with those in a turbulent channel flow and the predictions obtained by using rapid distortion theory. Our findings are recapitulated below.

(i) Considerable similarity in the instantaneous structures and statistical correlations is found between a homogeneous shear flow and a (inhomogeneous) channel flow at comparable shear-rate parameter, $S^* = Sq^2/\epsilon$.

(ii) It is shown that high shear rate alone, without the wall, can produce the streaky structures similar to those observed in the viscous sublayer of turbulent boundary layers.

(iii) High shear rate produces, in the limit of large total shear, a 'one-component' velocity field and a 'two-component' vorticity field. The development of anisotropy in the Reynolds-stress and vorticity fields is fairly well predicted by RDT.

(iv) It is demonstrated that RDT contains the essential mechanism responsible for development of turbulence structures in the presence of high shear rate, typical of the near-wall region in a turbulent shear flow.

The present study has shown similarity in statistics and instantaneous structures between the viscous sublayer in a wall-bounded turbulent flow and the homogeneous turbulent flow at high shear rate. Examination of the flow dynamics is necessary to establish the role of streaks in turbulence production. Since the basic mechanism for generating streaks is associated essentially with the presence of high shear rate and such a mechanism is accurately contained in RDT, a further study using RDT of dynamics of the streaks and modelling of the near-wall turbulence should provide insight into the generating mechanism.

Homogeneous shear flow and (inhomogeneous) turbulent channel flow are perceived to have very different characteristics. The similarity demonstrated in the present work, however, suggests a certain degree of universality among all shear flows. This is contrary to the common belief that it is unlikely that a universal model for different turbulent flows can be found. On the other hand, this study provides some support for the current modelling procedure (e.g. Lumley 1978) that assumes universality of local turbulence structures. The key element in constructing such a model hinges on identifying dimensionless parameters such as S^*. In order to accurately match turbulence statistics of a homogeneous flow with those of an inhomogeneous flow, one may have to devise additional parameters such as the 'effective total strain'. For instance, a refined model proposed by Townsend (1970) uses the effective total strain to account for the differences in non-uniformity of statistics in space and time. In his model, the effective total strain was modelled by defining an 'effective viscosity'. Equality of these parameters in different shear flows could guarantee similarity in turbulence statistics as well as in instantaneous flow structures.

The main conclusions of this work were presented at the Sixth Symposium on Turbulent Shear Flows, Toulouse, France in September, 1987 (Lee, Kim & Moin 1987).

We are grateful to R. S. Rogallo for many fruitful discussions. M. J. L. wishes to acknowledge the support of the National Research Council (NRC) Fellowship Program during a portion of this study.

Appendix. Turbulence lengthscales in shear flows

Because mean shear has a direct effect on large-scale eddies in a turbulent shear flow, it is appropriate to represent its effect as the ratio of the timescale of energy-containing eddies (l/q) to that of mean shear ($1/S$). It then remains to determine what lengthscale should be selected for use in the dimensionless shear-rate parameter, Sl/q. The most important criterion would be whether the magnitude of the resulting shear-rate parameter is capable of distinguishing different turbulence structures. For example, in a turbulent channel flow where the nature of turbulent eddies changes significantly between $y^+ \approx 10$ and 50, the suitable candidate should also exhibit a significant variation. In turbulent shear flows, some candidates for l include (i) the Prandtl's 'mixing length', l_m (see Hinze 1975, §5.2); (ii) the vertical scale of the uv-correlations, $L_{uv}^{(y)}$; and (iii) the 'dissipation length', $l_d = q^3/\epsilon$. Here, we examine how these lengthscales represent differences in turbulence structures of homogeneous turbulent flows at different shear rates (weak shear, Rogers & Moin 1987; strong shear, the present simulation) and at different locations in a turbulent channel flow (Kim *et al.* 1987).

The mixing length is defined as

$$-\overline{uv} = \nu_T S, \quad \nu_T = v' l_m \tag{A 1}$$

where $S = \mathrm{d}U/\mathrm{d}y$, or

$$l_m = \frac{-\overline{uv}}{Sv'}. \tag{A 2}$$

The resulting shear-rate parameter is then $S_m^* = -\overline{uv}/(qv')$. Figure 18 shows a slow variation of S_m^* with the vertical distance in a turbulent channel flow as well as with the total shear in homogeneous shear flow, except very close to the wall ($y^+ \leqslant 5$) and in the initial transient period ($\beta \leqslant 4$), respectively. In the channel flow, the variation is less than 20% for $10 \leqslant y^+ \leqslant 50$; in homogeneous shear flow, values of S_m^* at two much different shear rates are not significantly different. Thus, S_m^* is not capable of distinguishing different turbulence structures.

The vertical scale of the turbulent shear stress (uv) was computed from the two-point cross-correlations of u and v made dimensionless by the r.m.s. values. For the channel flow, the lengthscale, $L_{uv}^{(y)}$, was estimated to be the separation distance at which the arithmetic mean of the correlations, $\frac{1}{2}[Q_{uv}^*(y,y') + Q_{vu}^*(y,y')]$, drops to 0.05. This correlation value corresponds to about 10% of the peak value at $y = y'$, because the peak value (i.e. the correlation coefficient of uv) is about 0.5 in the near-wall region, $5 \leqslant y^+ \leqslant 50$. For homogeneous shear flow, the integral scale defined by $L_{uv}^{(y)} = \pi E_{uv}(\kappa_y = 0)/(-\overline{uv})$ was used. Figure 19 shows that in the turbulent channel the resulting shear-rate parameter, $S_{uv}^* = SL_{uv}^{(y)}/q$, varies very rapidly in the sublayer ($y^+ \leqslant 20$) and levels off away from the wall. In the homogeneous flow at a low shear rate, S_{uv}^* seems to reach an asymptotic value of about 2 for large total shear. In the presence of a high shear rate, S_{uv}^* appears to decrease with the total shear towards the value of the weak-shear case, a behaviour not desirable as the structural parameter.

The dissipation length, $l_d = q^3/\epsilon$, can be regarded as the lengthscale associated with 'energy-containing' eddies of turbulence in equilibrium. Figure 20 shows the

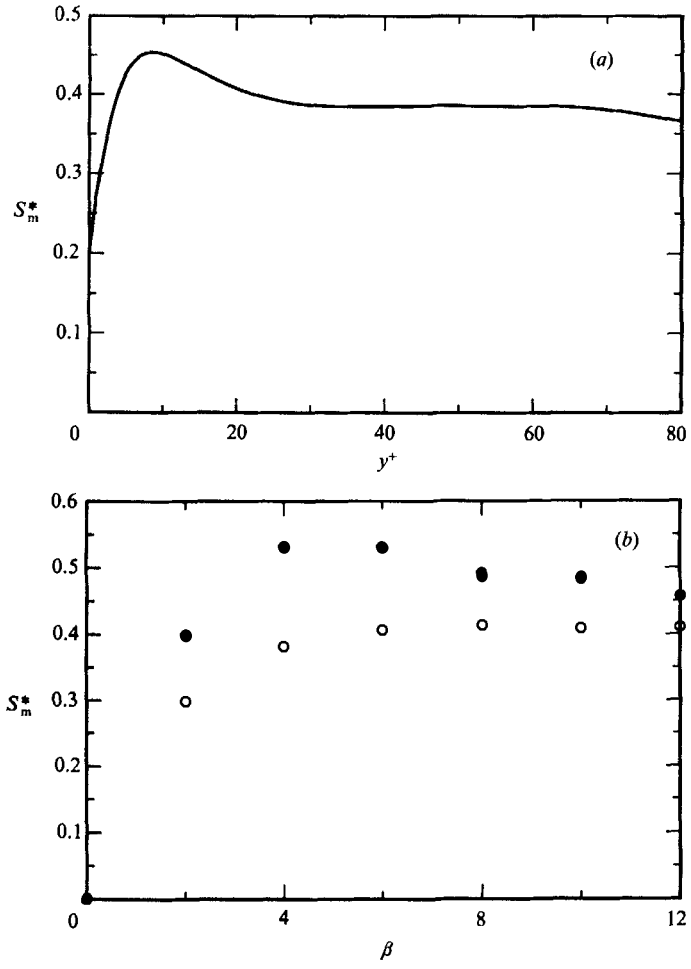

FIGURE 18. Behaviour of a shear-rate parameter, $S_m^* = Sl_m/q$, based on the Prandtl's mixing length, $l_m = -\overline{uv}/(Sv')$. (*a*) S_m^* *vs.* y^+ in a turbulent channel; (*b*) S_m^* *vs.* β in homogeneous turbulent flows at different shear rates: ○, low shear-rate case ($S_0^* \approx 5$); ●, high shear-rate case ($S_0^* \approx 34$).

evolution of the resulting shear-rate parameter, $S_d^* = Sl_d/q = Sq^2/\epsilon$, in homogeneous shear flows. It is apparent that a strong shear produces a much higher value of S_d^*. The profile of S_d^* in the turbulent channel (figure 1) shows that S_d^* is much higher in the sublayer than in the logarithmic layer, where the respective turbulence structures, i.e. streaks and hairpins, are markedly different. It may appear inappropriate to use the lengthscale that derives from the concept of equilibrium turbulence to describe homogeneous, sheared turbulence evolving in time. Nevertheless, S_d^* correctly indicates the dependence of turbulence structures on mean shear both in a channel flow and in homogeneous shear flows. Therefore, in this study we use S_d^* as the primary indicator of the type of turbulence structures, in the absence of a better choice.

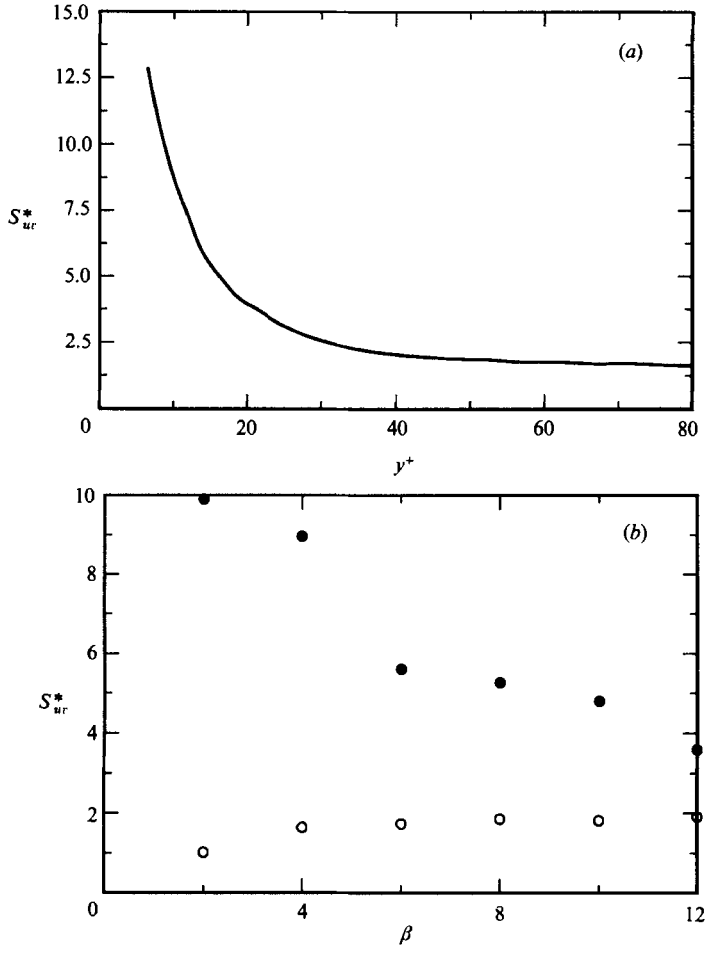

FIGURE 19. Behaviour of a shear-rate parameter, $S^*_{uv} = SL^{(y)}_{uv}/q$, based on the vertical scale of uv, estimated from the two-point cross-correlations of u and v. (*a*) S^*_{uv} *vs.* y^+ in a turbulent channel; (*b*) S^*_{uv} *vs.* β in homogeneous turbulent flows at different shear rates: ○, low shear-rate case ($S^*_0 \approx 5$); ●, high shear-rate case ($S^*_0 \approx 34$).

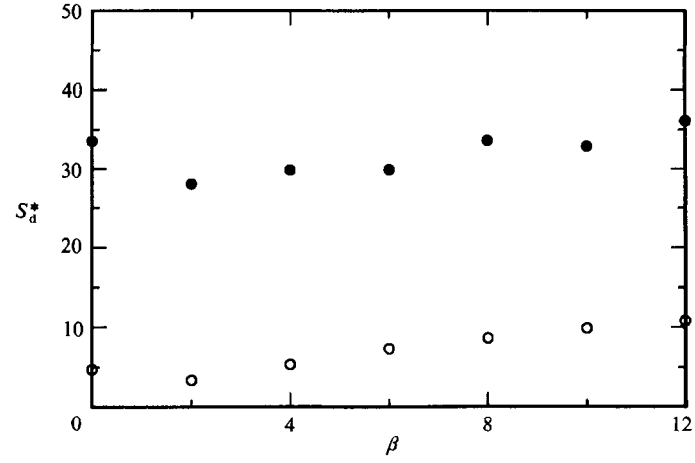

FIGURE 20. Evolution of a shear-rate parameter, $S^*_d = Sl_d/q$, based on the dissipation length, $l_d = q^3/\epsilon$, in homogeneous turbulent flows at different shear rates: ○, low shear-rate case ($S^*_0 \approx 5$); ●, high shear-rate case ($S^*_0 \approx 34$). (See figure 1 for the profile of S^*_d in a turbulent channel flow.)

REFERENCES

HEAD, M. R. & BANDYOPADHYAY, P. 1981 New aspects of turbulent boundary layer structure. *J. Fluid Mech.* **107**, 297–338.

HINZE, J. O. 1975 *Turbulence*. McGraw-Hill.

HUNT, J. C. R. 1978 A review of the theory of rapidly distorted turbulent flows and its applications. *Fluid Dyn. Trans.* **9**, 121–152.

HUNT, J. C. R. 1984 Turbulence structure in thermal convection and shear-free boundary layers. *J. Fluid Mech.* **138**, 161–184.

HUNT, J. C. R. & GRAHAM, J. M. R. 1978 Free-stream turbulence near plane boundaries. *J. Fluid Mech.* **84**, 209–235.

KIM, H. T., KLINE, S. J. & REYNOLDS, W. C. 1971 The production of turbulence near a smooth wall in a turbulent boundary layer. *J. Fluid Mech.* **50**, 133–160.

KIM, J. & MOIN, P. 1986 The structure of the vorticity field in turbulent channel flow. Part 2. Study of ensemble-averaged fields. *J. Fluid Mech.* **162**, 339–363.

KIM, J., MOIN, P. & MOSER, R. D. 1987 Turbulence statistics in fully developed channel flow at low Reynolds number. *J. Fluid Mech.* **177**, 133–166.

KLINE, S. J., REYNOLDS, W. C., SCHRAUB, F. A. & RUNSTADLER, P. W. 1967 The structure of turbulent boundary layers. *J. Fluid Mech.* **30**, 741–773.

LANDAHL, M. T. 1977 Dynamics of boundary layer turbulence and the mechanism of drag reduction. *Phys. Fluids* **20**, S55–S63.

LANDAHL, M. T. 1980 A note on an algebraic instability of inviscid parallel shear flows. *J. Fluid Mech.* **98**, 243–251.

LEE, M. J. 1985 Numerical experiments on the structure of homogeneous turbulence. Ph.D. thesis, Stanford University.

LEE, M. J. 1989 Distortion of homogeneous turbulence by axisymmetric strain and dilatation. *Phys. Fluids* A **1**, 1541–1557.

LEE, M. J. & HUNT, J. C. R. 1989 The structure of sheared turbulence near a plane boundary. In *Seventh Symp. on Turbulent Shear Flows, Stanford University, Stanford, California, Aug. 21–23, 1989* (ed. F. Durst, *et al.*), pp. 8.1.1–8.1.6.

LEE, M. J., KIM, J. & MOIN, P. 1987 Turbulence structure at high shear rate. In *Sixth Symp. on Turbulent Shear Flows, Toulouse, France, Sept. 7–9, 1987* (ed. F. Durst *et al.*), pp. 22.6.1–22.6.6.

LUMLEY, J. L. 1978 Computational modeling of turbulent flows. *Adv. Appl. Mech.* **18**, 123–176.

MOFFATT, H. K. 1967 The interaction of turbulence with strong wind shear. In *Atmospheric Turbulence and Radio Wave Propagation, Proc. Intl Colloq., Moscow, June 15–22, 1965* (ed. A. M. Yaglom & V. I. Tatarsky), pp. 139–156. Moscow: Nauka.

MOIN, P. & KIM, J. 1982 Numerical investigation of turbulent channel flow. *J. Fluid Mech.* **118**, 341–377.

MOIN, P. & KIM, J. 1985 The structure of the vorticity field in turbulent channel flow. Part 1. Analysis of the vorticity fields and statistical correlations. *J. Fluid Mech.* **155**, 441–464.

REYNOLDS, A. J. & TUCKER, H. J. 1975 The distortion of turbulence by general uniform irrotational strain. *J. Fluid Mech.* **68**, 673–693.

ROGALLO, R. S. 1981 Numerical experiments in homogeneous turbulence. *NASA Tech. Memo.* 81315.

ROGERS, M. M. & MOIN, P. 1987 The structure of the vorticity field in homogeneous turbulent flows. *J. Fluid Mech.* **176**, 33–66.

SMITH, C. R. & METZLER, S. P. 1963 The characteristics of low-speed streaks in the near-wall region of a turbulent boundary layer. *J. Fluid Mech.* **129**, 27–54.

TAVOULARIS, S., BENNETT, J. C. & CORRSIN, S. 1978 Velocity-derivative skewness in small Reynolds number, nearly isotropic turbulence. *J. Fluid Mech.* **88**, 63–69.

TENNEKES, H. & LUMLEY, J. L. 1972 *A First Course in Turbulence*. MIT Press.

THEODORSEN, T. 1952 Mechanism of turbulence. In *Proc. Second Midwestern Conf. on Fluid Mech., The Ohio State Univ., March 17–19, 1952 (Bulletin No. 149)* (ed. R. W. Powell, S. M. Marco & A. N. Tifford), pp. 1–18. Engng. Experiment Station, The Ohio State University.

THEODORSEN, T. 1955 The structure of turbulence. In *50 Jahre Grenzschichtforschung* (ed. H. Görtler & W. Tollmien), pp. 55–62. Braunschweig: Friedr. Vieweg & Sohn.

THOMAS, N. H. & HANCOCK, P. E. 1977 Grid turbulence near a moving wall. *J. Fluid Mech.* **82**, 481–496.

TOWNSEND, A. A. 1970 Entrainment and the structure of turbulent flow. *J. Fluid Mech.* **41**, 13–46.

TUCKER, H. J. & REYNOLDS, A. J. 1968 The distortion of turbulence by irrotational plane strain. *J. Fluid Mech.* **32**, 657–673.

UZKAN, T. & REYNOLDS, W. C. 1967 A shear-free turbulent boundary layer. *J. Fluid Mech.* **28**, 803–821.

WALLACE, J. M. 1982 On the structure of bounded turbulent shear flow: a personal view. In *Developments in Theoretical and Applied Mechanics*, vol. 11 [Selected papers of the *Eleventh Southeastern Conf. on Theoret. and Appl. Mech., Univ. of Alabama, Huntsville, April 8–9, 1982*] (ed. T. J. Chung & G. R. Karr), pp. 509–521. Dept. of Mech. Engng., University of Alabama at Huntsville.